



1 **What caused the interdecadal shift of the ENSO impact** 2 **on dust mass concentration over northwestern South Asia?**

3 Lamei Shi ^{1, 2}, Jiahua Zhang ^{1, 2}, Fengmei Yao ², Da Zhang ^{1, 2}, Jingwen Wang ^{1, 2},
4 Xianglei Meng², Yuqin Liu³

5 ¹ Key Laboratory of Digital Earth Science, Aerospace Information Research Institute, Chinese Academy
6 of Sciences, Beijing 100094, China

7 ² College of Earth and Planetary Sciences, University of Chinese Academy of Sciences, Beijing 101407,
8 China

9 ³ Key Laboratory of Urban Environment and Health, Institute of Urban Environment, Chinese Academy
10 of Sciences, Xiamen 361021, China

11 *Correspondence to:* Jiahua Zhang (zhangjh@radi.ac.cn)

12 **Abstract.** The change of large-scale circulation, especially El Niño-Southern Oscillation (ENSO), play
13 an important role in the interdecadal variability of dust activities over the dust source and downwind
14 regions. However, the detailed factors that lead to the interdecadal variability of the ENSO impact on
15 dust activities over the northwestern South Asia remain less clear, although previous studies have
16 discussed the response of the interannual dust activities over the northwestern South Asia to the ENSO
17 circle. Based on the linear regression model and MERRA-2 atmospheric aerosol reanalysis data, this
18 study investigated the interdecadal variability of the ENSO impact on dust activities as well as the
19 associated possible atmospheric drivers under two different warming phases over the northwestern South
20 Asia. Results indicated that the relationship between ENSO and surface dust mass concentration
21 (DUSMASS) experienced an obvious shift from the accelerated global warming period (1982–1996) to
22 the warming hiatus period (2000–2014). The change of Atlantic SSTA pattern weakened the impact of
23 ENSO on dust activities over the northwestern South Asia, while that of Indian Ocean SSTA pattern and
24 PDO tended to strengthen ENSO's effect. Both the Atlantic and Indian Ocean SSTA patterns were
25 modulated by the duration of ENSO events (i.e., continuing and emerging ENSO). The Eurasian
26 continent and Indian Ocean thermal contrast was less likely to cause the shift of ENSO–DUSMASS
27 relationship. This study provides new sights to numerical simulation involving the influence of
28 atmospheric teleconnections on the variability of dust activities and their influence mechanisms.

29 **Keywords:** Surface dust mass concentration; ENSO–DUSMASS relationship; interdecadal change;
30 large-scale atmospheric circulation; northwestern South Asia



1 Introduction

Dust aerosol is attracting an increasing concern due to its adverse impacts on human health (Bozlaker et al., 2013; Chen et al., 2004; Erel et al., 2006; Kaiser and Granmar, 2005; Poulsen et al., 1995; Sanchez de la Campa et al., 2013; Schulz et al., 2012) and environmental problems (Avila, 1998; Behrooz et al., 2017; Razakov and Kosnazarov, 1996). The Northwest Indian subcontinent, which is the most arid and semiarid area of South Asia, suffers heavy and frequent dust storms in summer due to extremely dry climate and strong winds (Jin and Wang, 2018). Those dust storms can travel long-distance to North India and the Arabian Sea, degrading air quality (Mahowald et al., 2010) and modifying ocean biogeochemistry processes (Richon et al., 2018; Singh et al., 2008). Particularly, dust aerosols can change local radiation budget, circulations, and Indian summer monsoon rainfall through absorption and scattering of solar radiation. The mineral dust over the northwestern South Asia is closely associated with the long-term variation of global climate (Banerjee et al., 2019; Bollasina et al., 2011; Jin et al., 2018). To better understand such feedback, and so that to give early warning to reduce disasters and losses caused by dust events, it is important to find out the controlling factors of the surface dust mass concentration (DUSMASS) and its long-term variation.

ENSO, as a periodic fluctuation in sea surface temperature (SST) and the air pressure across the equatorial Pacific Ocean, is as the primary large-scale driver of dust loading over the global dust source region (Trenberth et al., 2014). The Niño index significantly impacts the dust activity over the South Asia either indirectly through dust transport from Southwest Asia and/or directly through precipitation effect on dust emission (Banerjee et al., 2019; Bollasina et al., 2011; Jin et al., 2018).

An interdecadal climate regime shift was observed in the large-scale boreal winter circulation pattern over the North Pacific in the mid-1970s (Graham, 1994; Nitta and Yamada, 1989; Trenberth and Hurrell, 1994). Another remarkable climate change was observed in the early 21st century, i.e., an accelerated global warming prevailed before late 1990s and a warming hiatus dominated after that (Easterling and Wehner, 2009; Fyfe et al., 2011, 2013). After 2013, the global warming came to an end due to a persistent warm condition over the equatorial Pacific between Mar. 2014 and May 2016 (Hu and Fedorov, 2017). Concurrent with the Pacific climate shift, the large-scale circulation pattern and their atmospheric teleconnection also exhibit interdecadal change. Statistically 1980–1999 was characterized by a predominance of eastern equatorial Pacific (EP) and continuing (CT) El Niño event (McPhaden et



60 al., 2011; Yang and Huang, 2021), while the central equatorial Pacific (CP) and emerging (EM) El Niño
61 became more frequent since the beginning of the 21st century (Yang and Huang, 2021). The tropical
62 Pacific and Indian Ocean SST showed a rapid shift from a cold to warm state around the late 1970s. This
63 climate regime shift altered the links of ENSO with Indian summer monsoon rainfall (ISMR) (Kumar et
64 al., 1999). The changes of the teleconnection relationship at the turning point of mid-1970s have been
65 well documented, while that occurred around the early 21st century, particularly the effect of ENSO on
66 DUSMASS over the northwestern South Asia, is insufficiently analyzed.

67 The impact of ENSO on DUSMASS over the northwestern South Asia experiences interdecadal
68 shift. In the context of global warming (Deser et al., 2017; Kosaka and Xie, 2016), the relationship
69 between El Niño and monsoon experiences interdecadal change. The correlation between El Niño and
70 rainfall over India turned to be insignificant from the late 1970s, simultaneously, the relationship between
71 ENSO and monsoon also weakened around this turning point (Kumar et al., 1999). Two influence
72 mechanisms are proposed to explain this weakened ENSO–monsoon relationship. One is the varied
73 location of Walker circulation that adjusts the monsoon rainfall over Indian region, the other is the
74 temperature change over Eurasia that modulates the land-sea thermal gradient. Besides, the impact of
75 Atlantic Ocean pattern on the monsoon circulation over the Indian Ocean became stronger since late
76 1970s as the influence of the tropical Pacific has reduced (Kucharski et al., 2007; Sabeerali et al., 2019;
77 Srivastava et al., 2019). This in-turn impacts the circulation responsible for dust uplift and transport.
78 Several studies show that the dust activities over the northwest Indian Ocean were also affected by the
79 Indian Ocean dipole, which modulated the ENSO-related moisture (Banerjee and Kumar, 2016).
80 However, Agrawal et al. (2017) indicated that whenever the relationship of ISMR with IOD is weaker
81 (stronger), it becomes stronger (weaker) with the ENSO index. The two types of ENSO are also found
82 to differ in their links with ISMR, i.e., the central equatorial Pacific El Niño (CP El Niño) shows higher
83 correlation with Indian droughts than the eastern equatorial Pacific El Niño (EP El Niño) (Kumar et al.,
84 2006). In addition, the Pacific Decadal Oscillation (PDO) is reported to amplify the effect of ENSO when
85 it is in phase with ENSO (Roy et al., 2003).

86 In short, ENSO primarily influences the DUSMASS over the northwestern South Asia by impacting
87 the winter precipitation and the subsequent soil moisture, but the effects of ENSO on ISMR experienced
88 remarkable interdecadal change and many factors may cause this transition. Till now, however, the
89 interdecadal variability in the links of DUSMASS over the northwestern South Asia with ENSO has not



90 been investigated in detail compared to the North African and West Asian counterpart (Yu et al., 2015).
91 In addition, though many factors were proved to influence the short-term (e.g., interannual scale)
92 variation of the relationship between ENSO and dust activities over South Asia, their effects on the long-
93 term (e.g., interdecadal scale) change were still unclear. Cai et al. (2014) pointed out that global warming
94 will have a significant impact on ENSO. The extreme El Niño events will become more frequent under
95 the changes of atmospheric convection in the next half of the 21st century. Thus, understanding the
96 physical mechanism of the shift of the ENSO–DUSMASS relationship is of profound implications for
97 the forecast of dust trend in the future climate change scenario.

98 Many of the past researches on dust events were based on the aerosol optical depth (AOD) data
99 provided either by observational data at meteorological stations, which are sparsely distributed in the key
100 dust sources, or by satellite remote sensing with limited coverage and bias caused by cloud contamination
101 and uncertainty in retrieval algorithms, respectively (Zhang and Reid, 2009). Due to these limitations,
102 some of conclusions on the effect of ENSO events on dust activities remained contradictory. The current
103 study used the Modern-Era Retrospective Analysis for Research and Applications, version 2 (MERRA-
104 2) (Gelaro et al., 2017) atmospheric aerosol reanalysis data. The MERRA-2 can provide high-quality
105 dust aerosol variables related to emission, transport, and deposition process benefiting from the
106 integrated multiple satellite systems and ground-based AERONET (Randles et al., 2017). Another
107 advantage of MERRA-2 is its continuity in both temporal and spatial coverage (Gelaro et al., 2017).
108 Those are of great significance to explore the interactions between DUSMASS and large-scale
109 atmospheric circulation.

110 This study aims to investigate the large-scale atmospheric factors that contribute to the interdecadal
111 variability of the ENSO impact on DUSMASS over the northwestern South Asia. The paper is organized
112 as follows. Section 2 describes the datasets and methods. Section 3 presents factors that influence the
113 interdecadal change of the relationship between DUSMASS and wintertime Niño-3 index. Section 4
114 discusses the deficiency and prospect of this study. The conclusions are given in Sect. 5.

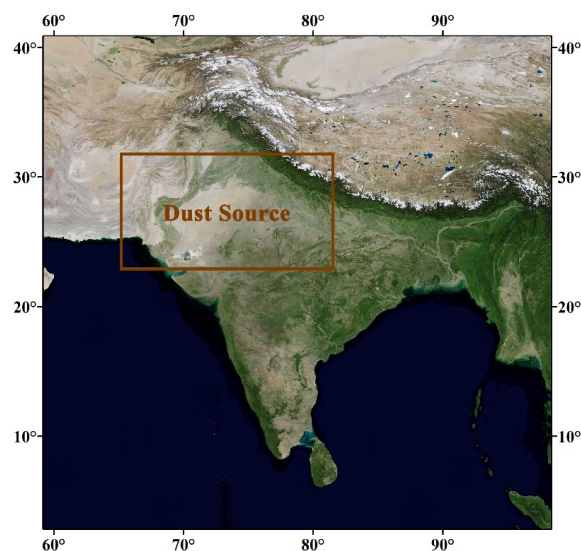
115 2 Data and methods

116 2.1 Study area

117 The main dust source over South Asia is a large arid region in the northwestern part of the Indian



118 subcontinent, which stretches from India to Pakistan. Most of the dust aerosols over this region come
 119 from the Thar desert. The southeastern part of the Thar desert lies between the Aravalli Hills. The desert
 120 extends to the Punjab Plain in the north and northeast, to the alluvial plains of the Indus River in the west
 121 and northwest, and to the Great Rann of Kutch along the western coast. The desert presents an undulating
 122 surface, with high and low sand dunes separated by sandy plains and low barren hills. The soils are
 123 mainly consisted by desert soils, red desertic soils, sierozems, the red and yellow soils of the foothills,
 124 the saline soils of the depressions, and the lithosols (shallow weathered soils) and regosols (soft loose
 125 soils) found in the hills. The subtropical desert climate here results from persistent high pressure and
 126 subsidence. The prevailing southwest monsoon winds from Indian Ocean that bring rain to much of the
 127 Indian subcontinent in summer tend to bypass the Thar to the east. The soils are generally infertile and
 128 overblown with sand due to severe wind erosion (Augustyn et al., 2019). The amount of annual rainfall
 129 in the desert is low, ranging from about 100 mm or less in the west to about 500 mm in the east. Almost
 130 90 % of the annual rainfall occurs in the season southwest monsoon, from July to September. While the
 131 prevailing wind is dry northeast monsoon during other seasons. Dust storms and dust-raising winds are
 132 common from May to July (Chauhan, 2003). Thus, the DUSMASS used in this study is averaged from
 133 June to July and May is neglected to weaken the disturbance of seasonal climatological differences.
 134 Analysis is carried out over the dust source in the northwestern South Asia (65° – 82° E, 24° – 32° N in Fig.
 135 1). All variables involving spatial average are taken from this region unless stated otherwise.





137 **Figure 1: Geographical map of South Asia (© Google Maps 2021). The dust source over the northwestern**
 138 **South Asia is marked with brown rectangle.**

139 2.2 Datasets

140 2.2.1 Dust concentration

141 Surface dust concentrations from 1982 to 2014 were provided by Modern-Era Retrospective
 142 Analysis for Research and Applications, version 2 (MERRA-2). MERRA-2 is produced via the Goddard
 143 Earth Observing System-Data Assimilation System (GEOS-DAS, version 5.12.4) based on GEOS-5
 144 climate model and the Gridpoint Statistical Interpolation (GSI) analysis scheme (Gelaro et al., 2017).
 145 Extensive satellite data are integrated into MERRA-2 to estimate dust concentration (Rienecker et al.,
 146 2011; Veselovskii et al., 2018). The dust products were comprehensively validated using the results of
 147 ground-based observation, satellite measurements, and numerical simulation (Rienecker et al., 2011).
 148 They have been widely applied to researches on global environment and climate change (He et al., 2019;
 149 Randles et al., 2017). The variable “Dust Surface Mass Concentration” (DUSMASS) with a spatial
 150 resolution of $0.625^{\circ} \times 0.5^{\circ}$ (longitude \times latitude) used in this study is from the dataset of
 151 “avgM_2d_aer_Nx”.

152 2.2.2 Land and sea surface temperature

153 To explore the possible influence of SST variability on the South Asian dust activity, we used three
 154 SST datasets from 1981 to 2014: (1) The National Oceanic and Atmospheric Administration (NOAA)
 155 Extended Reconstructed SST (ERSST) version 5 (Huang et al., 2017) that is available at $2^{\circ} \times 2^{\circ}$ spatial
 156 resolution is used for analysis, (2) Centennial in situ Observation-Based Estimates (COBE) version 2
 157 SST data at $1^{\circ} \times 1^{\circ}$ spatial resolution (Hirahara et al., 2014) and (3) Hadley Centre Global Sea Ice and Sea
 158 Surface Temperature (HadISST1.1) dataset produced by the Met Office, starting from 1870 up to the
 159 present with a horizontal resolution of $1^{\circ} \times 1^{\circ}$ (Rayner et al., 2003) are used for comparison. While the
 160 land-sea thermal contrast was calculated from the Hadley Centre Climate Research Unit Temperature
 161 version 5.0.1.0 (HadCRUT5) data from 1981 to 2014, which are a blend of the Climatic Research Unit
 162 land-surface air temperature dataset (CRUTEM5) and the Hadley Centre sea-surface temperature
 163 (HadSST4) dataset (Osborn et al., 2021). The longitude and latitude of SST index involved in this study
 164 were shown in Table 1.



Table 1: Longitude and latitude of SST index used in this study.

Acronyms	Full Name	Longitude and Latitude	Involved Ocean
Niño-3	—	150°–90° W, 5° S–5° N	Pacific
Niño-3.4	—	170°–120° W, 5° S–5° N	Pacific
Niño-4	—	160° E–150° W, 5° S–5° N	Pacific
ASGI	Atlantic SSTA gradient index	North: 60°–30° W, 0–20° N	Atlantic
		South: 20° W–10° E, 0–20° S	Ocean
TWISSTA	Tropical western Indian ocean SSTA	50°–70° E, 10° S–15° N	Indian Ocean
PDO	Pacific decadal oscillation	117.5° E–77° W, 20°–66.5° N	Pacific

2.2.3 Large-scale climate indices

Three monthly Niño indices Niño-3, Niño-3.4, and Niño-4 from 1981 to 2014, which monitor the SST anomalies averaged across the eastern equatorial Pacific, Pacific from dateline to the South American coast, and central equatorial Pacific, respectively, were used to analyze their links with DUSMASS over the northwestern South Asia. Kinter et al. (2002) pointed out that Nov.–Jan. is the peak season for El Niño/La Niña, thus the average Niño index from (–1) Nov. to (0) Jan. was used. Only one Niño index that shows the highest correlation coefficient was retained in this study, i.e., Niño-3. The large-scale climate indices, such as PDO, was also used to explore the potential factors that contributed to the interdecadal shift of ENSO–DUSMASS relationship. All those indices were from the Climate Predict Center of National Oceanic and Atmospheric Administration (NOAA/CPC).

2.3 Method

In this study, we compared the impact of ENSO on DUSMASS over the northwestern South Asia under two different warming epochs, and investigate the potential global change drivers to the shift of ENSO–DUSMASS relationship. The global warming is separated into the accelerated warming period from 1982 to 1996 and the warming hiatus period from 2000 to 2014. The year 2014 was added to the warming hiatus period to keep the length of those two periods consistent. This classification is not controversial since the ENSO year stated in this study spanned from antecedent November to current



183 January.

184 2.3.1 Contribution of factors to relationship

185 The contribution of Z (Indian Ocean SSTA variance, Atlantic SSTA gradient index, or Eurasian
 186 continent and Indian Ocean thermal contrast) modifying ENSO–DUSMASS relationship was defined as:
 187 sliding regression of Z onto Niño-3 index multiplies by sliding regression of DUSMASS onto Z with
 188 Niño-3 removed (Yang and Huang, 2021).

189 2.3.2 Signal removal method

190 The residual time series based on the linear regression method were used to remove the ENSO signal
 191 in the oceanic SSTA pattern, (Yang and Huang, 2021), as shown in Eq. (1):

$$\xi_{remove} = \xi - Z \times \frac{cov(\xi, Z)}{var(Z)} \quad (1)$$

192 Where ξ and Z is the time series of oceanic SSTA (such as Atlantic and Indian Ocean) and ENSO,
 193 respectively, cov indicated the covariance between two variables, and var indicates the variance of
 194 ENSO.

195 2.3.3 Coupled spatial pattern analysis

196 The maximum covariance analysis (MCA) is a useful tool for isolating the most coherent pairs of
 197 spatial patterns and their associated time series by performing an eigenanalysis on the temporal
 198 covariance matrix between two geophysical fields (Storch and Zwiers, 1999). The MCA method was
 199 used to analyze the coupled patterns between DUSMASS and oceanic SSTA.

200 2.3.4 Definition of different types of ENSO

201 Following Yeh et al. (2009), an El Niño event is defined as CP El Niño if Niño-4 > Niño-3 and
 202 Niño-3.4 > 0.5°C, and as EP El Niño if Niño-4 < Niño-3 and Niño-3.4 > 0.5°C. Similarly, a La Niña
 203 event is referred to as CP La Niña if Niño-4 < Niño-3 and Niño-3.4 < -0.5°C, and as EP La Niña if Niño-
 204 4 > Niño-3 and Niño-3.4 < -0.5°C. According to this method, the CP El Niño years during 1982–2014
 205 include 1988, 1991, 1995, 2003, 2005, 2007, and 2010; CP La Niña years include 1984, 1989, 1999,
 206 2001, 2011, and 2012; EP El Niño years include 1983, 1987, 1992, and 1998; EP La Niña years include
 207 1985, 1996, 2000, and 2008.



208 Following Yang and Huang (2021), the EM and CT ENSO were defined based on the Niño-3 index.
 209 For CT ENSO, the Niño-3 index follows the rule of $[(−1)\text{Oct.}−(0)\text{Jan.}]_{\text{mean}} > 0.5 (< −0.5)\text{STD} \&$
 210 $[(0)\text{Mar.}−(0)\text{May}] > 0.5 (< −0.5)\text{STD} \& [(0)\text{Jun.}−(0)\text{Sep.}] > 0 (< 0)$ or $[(−1)\text{Oct.}−(0)\text{May}] > 0.75$
 211 $(< −0.75)\text{STD} \& [(0)\text{Jun.}−(0)\text{Sep.}]_{\text{mean}} > 0.5 (< −0.5)\text{STD}$. To acquire more available samples in the
 212 study period, all the ENSO years that were not defined as CT ENSO were identified as EM ENSO year
 213 in this study, which was different from Yang and Huang (2021). Based on this definition, the CT El Niño
 214 years during 1982–2014 include 1982, 1983 and 1987; CT La Niña years include 1984, 1985, 1989, 1996,
 215 1999, 2000, and 2011; EM El Niño years include 1995, 1998, 2003, 2005, 2007, and 2010; EM La Niña
 216 years include 2008 and 2012.

217 The effect of ENSO type on the correlation between ENSO and DUSMASS was partly analyzed
 218 through the duration and intensity of Indian Ocean SSTA following the ENSO events. We calculated the
 219 correlation between the variance of monthly Indian Ocean SSTA from $(−1)$ Sep. to (0) May and
 220 DUSMASS. It is found that the maximum correlation between the Indian Ocean SST and Niño-3 SST
 221 occurs in the central Indian Ocean rather than in the Arabian Sea SST (Clark et al., 2000). Therefore, the
 222 variance of monthly Indian Ocean SSTA was calculated over the central Indian Ocean (tropical western
 223 Indian ocean, TWISSTA) $(50^{\circ}–70^{\circ}\text{E}, 10^{\circ}\text{S}–15^{\circ}\text{N})$. The EP ENSO tends to onset in spring (Mar.–May)
 224 and reaches the mature phase in winter, then decays near Apr. of the second year. Whereas the onset of
 225 CP ENSO appears in summer and reaches the peak around Dec. –Jan., then decays in early spring of the
 226 second year (Kao and Yu, 2009). Consequently, monthly Indian Ocean SSTA was taken from $(−1)$ Sep.
 227 to (0) May.

228 In this study, “ (0) month” represents the year concurrent with the year when DUSMASS is acquired
 229 and “ $(−1)$ month” represents the preceding year.

230 3 Results

231 3.1 Observed interdecadal change of the impact of Niño-3 index on DUSMASS

232 In the present study, we found that the ENSO–DUSMASS relationship experienced an interdecadal
 233 transition at around 1999/2000. Based on the 15-year sliding correlation from 1982 to 2014 (Fig. 3 (b)),
 234 the ENSO–DUSMASS relationship was weak before the end of 1990s and became stronger after that.
 235 Specifically, the winter Niño-3 index $((−1)\text{Nov.}−(0)\text{Jan.})$ presented a weakly negative relation with



DUSMASS during the accelerated warming period (1982–1996), while exhibited a significant negative correlation ($P < 0.01$) during the warming hiatus stage (2000–2014). The varied correlation was not influenced by the lengthen of sliding windows or the type of Niño index, and was confirmed by multiple datasets of SST (not shown).

3.2 Factors influencing the interdecadal change of the impact of Niño-3 index on DUSMASS

3.2.1 Tropical Atlantic SSTA pattern

With the global climate change observed in early 2000s, the ENSO-related tropical Atlantic SSTA experienced an obvious transition, i.e., from an Atlantic Niña pattern during 1982–1996 to an Atlantic Niño pattern during 2000–2014 (Fig. 2), which is also reported by Yang and Huang (2021). The tropical Atlantic SSTA pattern was a crucial factor for the restoration of ENSO–ISMR relationship since the late 1990s (Yang and Huang, 2021), thus, it could also disturb the impact of ENSO on dust activities over the northwestern South Asia. In order to validate the connection between the Atlantic SSTA and the DUSMASS–Niño-3 relationship, an Atlantic SSTA gradient index (ASGI) was used to describe the SSTA pattern shift in the tropical Atlantic, which represented the difference of averaged SSTA between tropical North Atlantic and tropical South Atlantic (marked by two rectangles in Fig. 2). The Atlantic Niña pattern develops and is most sensitive to ENSO in spring (Tokinaga et al., 2019), thus the SST averaged from Mar. to May was used in this section.

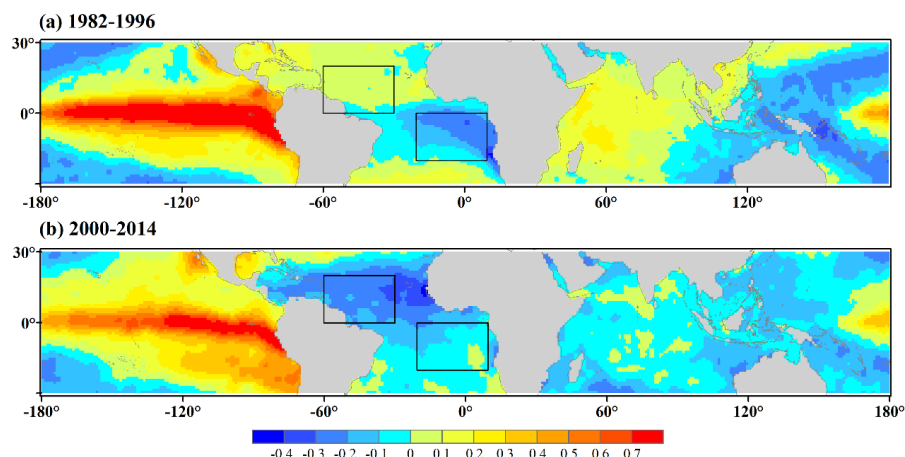


Figure 2: Regression of tropical SSTA onto Niño-3 index. Black rectangles denote the regions to define ASGI. The range of the upper one is 60–30° W, 0–20° N and that of the lower one is 20° W–10° E, 20–0° S. (Similar with Fig. 2 (c)–(d) of Yang and Huang (2021) but with different time spans)



Based on the 15-year sliding correlation during 1982–2014 (Fig. 3), the relationship between Niño-3 and ASGI witnessed a reversal at the early 2000s, simultaneously, the correlation between Niño-3 and DUSMASS exhibited the similar change. However, the significance of correlation between Niño-3 and DUSMASS in the two warming phases (1982–1996 and 2000–2014) was opposite to that between Niño-3 and ASGI, i.e., the correlation between Niño-3 and ASGI passed the 99 % confidence level during 1982–1996 and it did not pass the 95 % confidence level during 2000–2014, while the correlation between Niño-3 and DUSMASS showed a contrary trend with a higher correlation coefficient appeared in 2000–2014. Additionally, Figure 4 proved that during 1982–1996, ASGI weakened the DUSMASS–Niño-3 relationship while the contribution of ASGI was close to 0.0 during 2000–2014. All these clarified that the weakening of the influence of ASGI on Niño-3 index promoted the effect of Niño-3 index on DUSMASS.

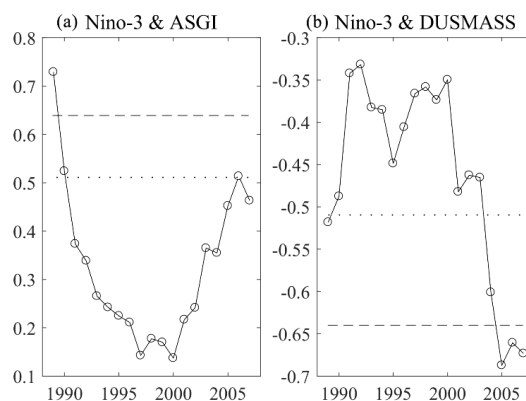
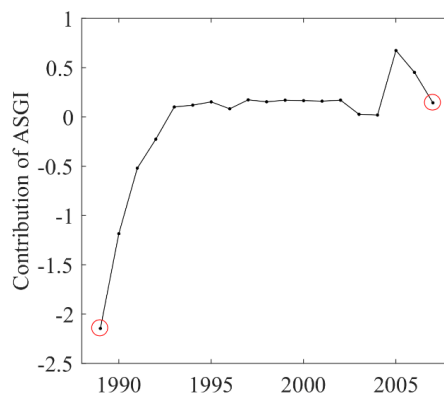


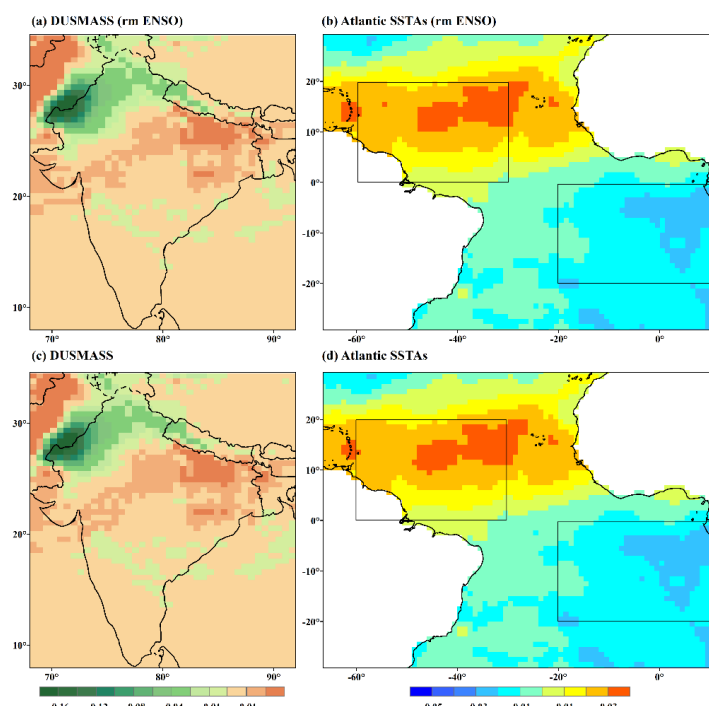
Figure 3: The 15-year sliding correlation between (a) Niño-3 and Atlantic SSTA gradient index (ASGI), (b) Niño-3 index and DUSMASS during 1982–2014. The x-axis denotes the middle year of the period under analysis. The horizontal dashed line and dotted line indicate the 99% and 95 % confidence levels respectively.





273 **Figure 4: Sliding contribution of Atlantic SSTA gradient index (ASGI) to ENSO–DUSMASS relationship. The**
 274 **two circles represented the 15-year window spanning from 1982 to 1996 and 2000 to 2014, respectively. The**
 275 **x-axis denotes the middle year of the period under analysis.**

276 To illustrate the spatial coupling pattern of Atlantic SSTA and DUSMASS, the MCA method was
 277 utilized. Figures. 5 (a)–(b) showed the correlation between DUSMASS and tropical Atlantic SSTA of the
 278 first MCA mode with ENSO-related signals removed. It is clear that the DUSMASS presented
 279 remarkable decrease over northern and northwestern India, meanwhile, the tropical Atlantic SSTA
 280 displayed an apparent dipole pattern with negative in the south and positive in the north.



281 **Figure 5: Spatial correlation between tropical Atlantic SSTA and DUSMASS of the first mode of the MCA**
 282 **analysis in 1982–2014. The first MCA mode of (a) the DUSMASS, and (b) the tropical Atlantic SSTA with**
 283 **ENSO-related signals removed. (c)–(d) As in (a)–(b), but for the original series including the ENSO signal.**

285 The MCA results with ENSO-related signals removed were similar with that including the ENSO-
 286 related signals (Figs. 5 (c)–(d)), demonstrating that ENSO exhibited no significant impact on the spatial
 287 coupling between DUSMASS and Atlantic SSTA. Besides, the regression of DUSMASS onto ASGI was
 288 close in 1982–1996 and 2000–2014 (not shown), which were both insignificant, suggesting no apparent
 289 interdecadal transition in the relationship between DUSMASS and Atlantic SSTA in recent decades. This
 290 manifested that the shift of the relationship between DUSMASS and ENSO was not due to the



interdecadal transition in the relationship between DUSMASS and Atlantic SSTA.

The MCA result indicated that the colder tropical South Atlantic could suppress dust storm over the northwestern South Asia but the warmer tropical South Atlantic could enhance the dust concentration. As reported previously (e.g., Kucharski et al., 2009, 2008, 2007; Kucharski and Joshi, 2017; Sabeerali et al., 2019; Yadav, 2016, 2009), the warm tropical North Atlantic and cold tropical South Atlantic were conducive for ISMR, which was bridged by the large-scale monsoon circulation (Rong et al., 2010), Rossby wave train (Yadav, 2009), Asian jet (Yadav et al., 2018), Kelvin wave response (Sabeerali et al., 2019), and an abnormal westerly. Considering the relationship between ISMR and tropical Atlantic SSTA, the Atlantic Niña pattern that was linked to ENSO in 1982–1996 (Fig. 2 (a)) tended to suppress dryness and weaken the positive relationship between DUSMASS and ENSO, while the Atlantic Niño pattern in 2000–2014 would decrease the north-south Atlantic SSTA gradient and offset the effect of Atlantic Niña pattern, which weakened the dryness's response to Atlantic and enhanced the ENSO–DUSMASS relationship. Accordingly, the correlation between ENSO and DUSMASS strengthened together with the change of Atlantic SSTA pattern.

It was reported that the interdecadal shift of tropical Atlantic SSTA pattern was a response to the multi-year ENSO events (Tokinaga et al., 2019). The multi-year ENSO event, which was also called as continuing ENSO (CT ENSO), was a situation where the summer ENSO SSTA continued from the preceding year. Another type of ENSO, which was called as emerging ENSO (EM ENSO), was characterized as late Atlantic SSTA response that started from June. The CT ENSO primarily dominated during 1982–1996, while 2000–2014 was dominated by EM ENSO (Yang and Huang, 2021). The impact of the two types of ENSO on the shift of the DUSMASS–Niño-3 relationship were examined. Table 2 showed that ASGI was significantly correlated with Niño-3 in the CT ENSO years, which was not observed in the EM ENSO years. Simultaneously, DUSMASS was significantly related to Niño-3 only in the EM ENSO years. The composite correlation changes for CT and EM ENSOs resembled that for ENSOs in 1982–1996 and 2000–2014, indicating that the shift of Atlantic SSTA pattern plays an important role in modulating the DUSMASS–Niño-3 relationship.

Table 2: Correlation between ASGI and Niño-3 as well as DUSMASS in two different phases (* and * indicate the correlations that are significant on a 0.1 and 0.01 level, respectively).**

R	CT ENSO	EM ENSO	1982–1996	2000–2014
---	---------	---------	-----------	-----------



ASGI & Niño-3	0.78 (***)	0.19	0.73 (***)	0.46 (*)
DUSMASS & Niño-3	-0.60 (*)	-0.75 (***)	-0.51 (*)	-0.67 (***)

319

320 Apart from the south-north dipole pattern of the tropical Atlantic SSTA, the switch in the intensity
 321 and location of North Atlantic SST tripole pattern was also responsible for the change of Niño-3–
 322 DUSMASS relationship (Banerjee et al., 2021). Compared with the global warming hiatus period, the
 323 North Atlantic SST exhibited higher correlation with dust activities over South Asia in the context of
 324 global warming, which was teleconnected through the precipitation and westerly anomalies over the
 325 Indo-Gangetic plain (Banerjee et al., 2021). Therefore, the impact of Niño-3 on DUSMASS was
 326 weakened during 1982–1996 when an accelerated global warming was witnessed, while the impact was
 327 stronger during 2000–2014 when a warming hiatus prevailed.

328 3.2.2 Variation of Indian ocean SST

329 Previous studies have recognized the covariability between the western Pacific and Indian Ocean
 330 (Kug et al., 2005; Wang et al., 2003; Watanabe and Jin, 2002). ENSO can affect the Indian Ocean SST
 331 in the form of Walker circulation and the Indian Ocean variability can also modulate the ENSO variability
 332 (Kug et al., 2005; Wu and Kirtman, 2004; Yu et al., 2002). It is known that ENSO mainly influences the
 333 monsoon rainfall of South Asia through changing the SST of Indian ocean (Krishnamurthy and Kirtman,
 334 2003; Srivastava et al., 2019). During CT ENSO years, the ENSO event in summer primarily starts from
 335 the preceding winter, while in EM ENSO years, the ENSO event mainly emerges in late spring (Yang
 336 and Huang, 2021). Correspondingly, the associated Indian Ocean SST oscillation also varies in these two
 337 different ENSO years. In order to explore whether the different types of La Niña impacted the
 338 DUSMASS over the northwestern South Asia through adjusting the duration of the temperature anomaly,
 339 we compared the SST and the variance of the monthly SSTA from (–1) Sep. to (0) May over the tropical
 340 western Indian ocean (central Indian Ocean, 10° S–15° N, 50–70° E).

341 Figure 6 showed that the variances in the EM La Niña years were generally larger than that in the
 342 CT La Niña years, while the variances in the EM El Niño years were generally smaller than that in the
 343 CT El Niño years. The monthly tropical western Indian ocean SSTA in CT and EM ENSO years were
 344 seen in Fig. S1, which showed that the monthly SSTA from preceding Sep. to following May appeared
 345 as persistent positive and negative anomalies in EM El Niño and CT La Niña years, respectively, while



those in EM La Niña and CT El Niño years experienced monthly and/or seasonal oscillatory. Concurrently, the difference of DUSMASS in El Niño and La Niña years was obvious in the EM ENSO period with higher values appeared in La Niña years (Fig. 7). However, in the CT ENSO period, no significant difference was observed between El Niño and La Niña years. Therefore, it is hypothesized that the EM ENSO conditions, which was associated with higher Indian Ocean SST variance, were more favorable to trigger the variation of DUSMASS. Yang and Huang (2021) reported that 1982–1996 was primarily dominated by CT ENSOs while EM ENSOs primarily controlled during 2000–2014. Combined with abovementioned hypothesis, the correlation between DUSMASS and Niño-3 should be higher in the later period 2000–2014, which was consistent with the interdecadal change of this relationship.

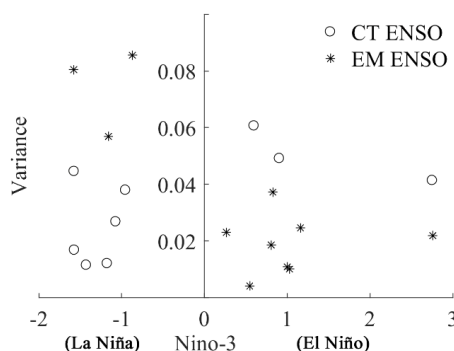


Figure 6: Scatter diagram between Niño-3 index and the variance of the monthly SSTA from (–1) Sep. to (0) May over the tropical western Indian ocean (50–70° E, 10° S–15° N) separately for continuing (CT) and emerging (EM) ENSO.

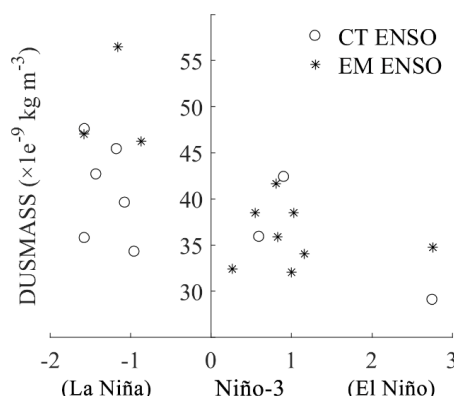


Figure 7: Scatter diagram between DUSMASS and Niño-3 index separately for continuing (CT) and emerging (EM) ENSO.

Unlike the weakening effect of tropical Atlantic SSTA pattern on the DUSMASS– Niño-3



relationship, the Indian Ocean SSTA variance, as a response to the type of ENSO, tended to strengthen this relationship since the impact of Indian Ocean SSTA variance was synchronous with that of Niño-3. The correlation coefficient between the variance of Indian Ocean SSTA and DUSMASS turned from 0.15 ($P > 0.1$) during 1982–1996 to 0.57 ($P < 0.05$) during 2000–2014, which was different from the insignificant regression of DUSMASS onto ASGI in those two periods. To quantify the role of Indian Ocean SSTA variance in modifying the DUSMASS–Niño-3 relationship, we calculated the contribution of SSTA variance to the relationship as shown in Fig. 8. The contribution of Indian Ocean SSTA variance was close to 0.0 in 1982–1996 and approached to 1.0 in 2000–2014, which further confirmed the strengthening effect of Indian Ocean SSTA in the later period.

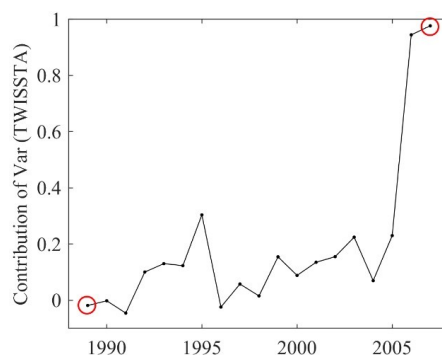
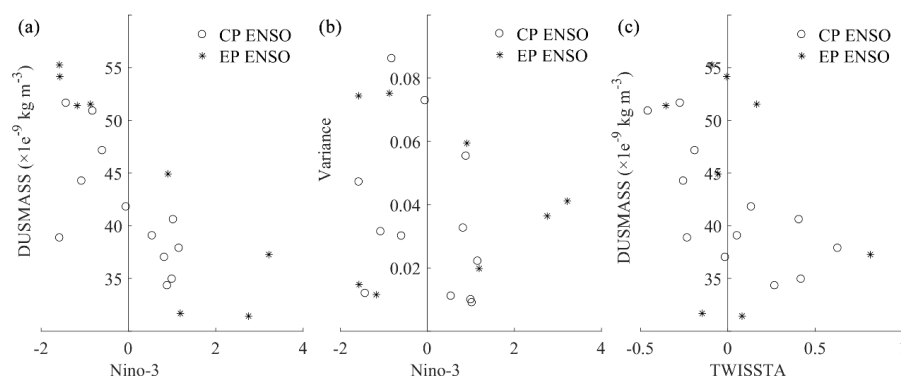


Figure 8: Sliding contribution of tropical western Indian Ocean SSTA (TWISSTA) variance to ENSO–DUSMASS relationship. The two circles represented the 15-year window spanning from 1982 to 1996 and 2000 to 2014, respectively. The Niño-3 index was multiplied by -1 considering that the higher variances in the later period corresponded to the negative phase of ENSO.

Apart from the CT ENSO and EM ENSO, the response of Indian Ocean SSTA was also different between CP ENSO and EP ENSO (Hu et al., 2018). It was reported that the onset of EP ENSO appears in spring and decays near Apr. of the second year, while the CP ENSO tends to onset in summer, reaches their peak intensity around December–January, and decays in early spring of the second year. The duration of the CP ENSO is about eight months shorter than that of the EP ENSO (Kao and Yu, 2009). Especially for the El Niño event, the maximum negative SSTA appears in the winter of year (+1) in the CP El Niño while a stronger cold anomaly appears in the winter of year (+2) in the EP El Niño, indicating a slow and strong cooling after the EP El Niño but a quicker and weaker cooling after the CP El Niño (Hu et al., 2012). In order to explore whether the different types of ENSO impacted the DUSMASS over northwestern South Asia through adjusting the Indian Ocean SST, we compared the SST and DUSMASS



387 in CP and EP ENSO conditions.



388
 389 **Figure 9: Scatter diagram between (a) Niño-3 and DUSMASS, (b) Niño-3 and TWISSTA variance, and (c)**
 390 **TWISSTA and DUSMASS separately for CP and EP ENSO.**

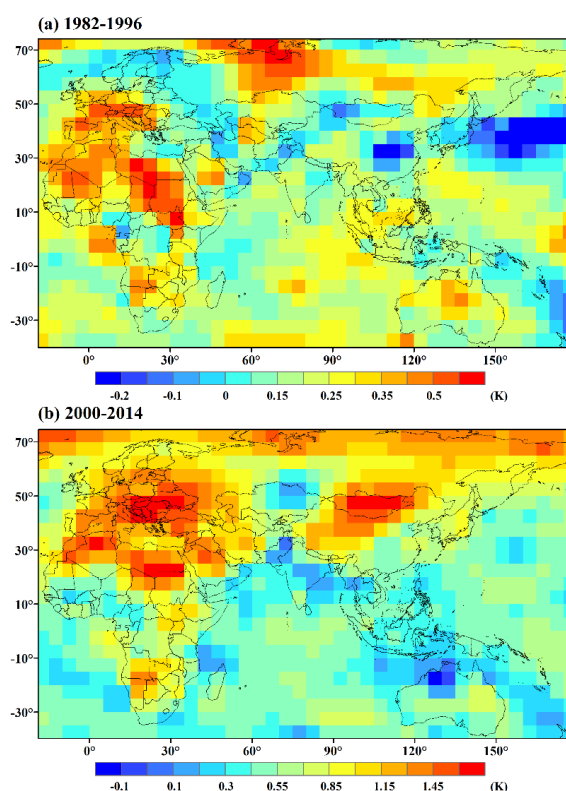
391 Figure 9 (a) showed that the DUSMASS was generally larger under La Niña conditions than that
 392 under El Niño conditions. Specifically, the mean DUSMASS in EP La Niña years was higher than that
 393 in CP La Niña years, however, this difference was not significant. In addition, no remarkable difference
 394 in Indian Ocean SSTA variance was observed under the two types of ENSO, as shown in Fig. 9 (b). The
 395 correlation analysis (not shown) revealed that the significant interdecadal variability of Niño-3–
 396 TWISSTA and DUSMASS–TWISSTA relationship was spotted in winter (averaged from (–1) Dec. to
 397 (0) Feb). Nevertheless, the TWISSTA under two types of ENSO and the DUSMASS in varied TWISSTA
 398 exhibited no significant differences (Fig. 9 (c)), indicating that the variation of TWISSTA and the
 399 response of DUSMASS to TWISSTA was not modulated by the types of EP and CP ENSO. The results
 400 demonstrated that the transition of EP and CP ENSO exhibited no significant contribution to the shift of
 401 the DUSMASS–Niño-3 relationship.

402 3.2.3 Eurasian continent and Indian Ocean thermal contrast

403 Kumar et al. (1999) pointed out that in El Niño events before 1980, colder Eurasian temperature
 404 anomalies coupled with positive Pacific SST anomalies coincides with negative ISMR anomalies. The
 405 inverse connection between ENSO and Indian summer monsoon is maintained. While in the El Niño
 406 events during 1981–1997, the increased premonsoon surface temperatures over Eurasia far exceeded the
 407 warming in the Indian Ocean. The stronger land-sea thermal contrast is conducive for a stronger monsoon,
 408 which overrides the influence of El Niño. The Eurasian temperature anomalies could also disturb the
 409 impact of ENSO on DUSMASS over the northwestern South Asia since monsoon and rainfall are crucial



410 factors to trigger dust storms. To isolate the role of Eurasian continent temperature anomalies in
 411 modulating the effect of ENSO on DUSMASS over the northwestern South Asia in the recent climate
 412 change (i.e., from an accelerated global warming during 1970s–1990s to a warming hiatus during 1998–
 413 2014), we compared the Eurasian continent (60°–100° E, 30°–45° N) and Indian Ocean (60°–100° E, 10°
 414 S–10° N) thermal contrast in those two periods and calculated its contribution to the change of ENSO–
 415 DUSMASS relationship.



416
 417 **Figure 10: Spatial distribution of summer surface temperature anomaly separately for 1982–1996 (a) and**
 418 **2000–2014 (b).**

419 Figure 10 displayed the spatial distribution of summer surface temperature. Compared to the spatial
 420 distribution of surface temperature during 1982–1996, the warming over Eurasian continent was
 421 significantly stronger than that over tropical Indian Ocean during 2000–2014, which indicated higher
 422 land-sea thermal contrast in the later period. The strong land-sea thermal contrast can significantly impact
 423 the drought conditions over the arid regions in the northwestern South Asia through adjusting the south
 424 Asian monsoon, moisture transmission, and precipitation (Kinter et al., 2002; Kumar et al., 1999).

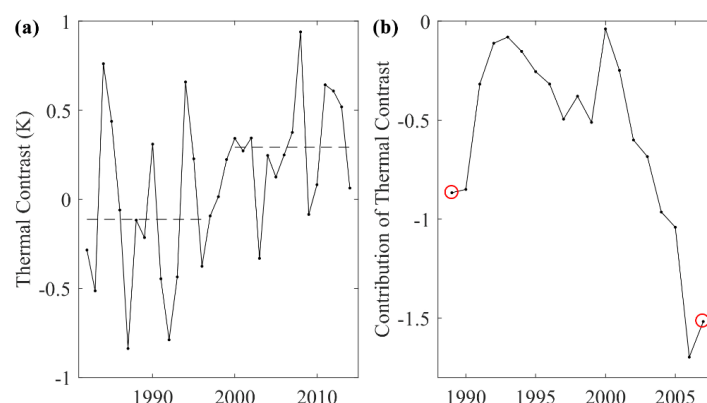


Figure 11: Time series of summer Eurasian continent and Indian Ocean thermal contrast. The dotted lines denote the average values from 1982 to 1996 and from 2000 to 2014, respectively; (b) Sliding contribution of Eurasian continent and Indian Ocean thermal contrast to ENSO–DUSMASS relationship. The circles represented the 15-year window spanning from 1982 to 1996 and from 2000 to 2014, respectively.

As shown in Fig. 11 (a), the Eurasian continent and Indian Ocean thermal contrast during 2000–2014 was higher than that in 1982–1996. As a result, the negative contribution of the thermal contrast grew stronger in the later period compared with that in the first period. The enhancement of thermal contrast’s effect mitigated the impact of Niño-3 index on DUSMASS, and this should have led to higher correlation coefficient in 1982–1996 rather than in 2000–2014, which conflicted with the observed interdecadal transition of DUSMASS–Niño-3 relationship. Thus, the change of Eurasian continent and Indian Ocean thermal contrast cannot explain the difference of DUSMASS–Niño-3 relationship in the varied warming phases.

3.2.4 Phase shift of Pacific Decadal Oscillation

It is suggested that the PDO can influence the interannual variability of ISMR by enhancing the ENSO–ISMR relationship when ENSO and the PDO are in-phase, while weakening the relationship when they are out of phase (Dong et al., 2018; Krishnamurthy and Krishnamurthy, 2014). However, it is unclear whether the PDO is responsible for the shift of the ENSO–DUSMASS relationship. Table 3 listed the years with different phases of ENSO and PDO as well as years when ENSO and PDO are in (out of) phase separately. The correlation coefficient between Niño-3 and DUSMASS and significance level were also given. It demonstrated that the PDO significantly strengthened the correlation between Niño-3 and DUSMASS as the coefficient turned from -0.34 ($P > 0.1$) when PDO and Niño-3 were out of phase to 0.71 ($P < 0.01$) when they were in-phase.



448 The 200 hPa velocity potential trend in the positive PDO years exhibited a decrease (divergence)
 449 over the western tropical Pacific and an increase (convergence) over the tropical Indian Ocean and Indian
 450 subcontinent (across 40°–100° E), as shown in Fig. 8 (a) of Huang et al. (2020). The upper-level
 451 convergence over India and the adjacent seas corresponded to the anomalous descending motion, which
 452 suppressed ISMR and consequently stimulated the dust storms over South Asia. Meanwhile, two
 453 anomalous anticyclones developed to the northwest and southwest of India due to the depressed
 454 convection (Huang et al., 2020). The westerlies on the northern flank of the northwest anticyclonic
 455 anomalies advected relatively drier air from the Eurasian continent (Parker et al., 2016) to the west of
 456 north-central India. Those situations were in favor of dust generation, in addition, the eastward transport
 457 of dust from Southwest Asia by the westerlies contributed about half of the dust concentration over the
 458 Indo-Gangetic plain (Banerjee et al., 2019). While in the negative PDO years, anomalous ascent appeared
 459 over India, which enhanced ISM convection and rainfall, as shown in Fig. 8 (b) of Huang et al. (2020).
 460 Similarly, two anomalous cyclones established to the west of India. The easterlies over the northern
 461 Indian subcontinent transported wet air from the Bay of Bengal into the east of north-central India, which
 462 increased rainfall and reduced dust emissions over the northern India (Huang et al., 2020). The
 463 descending and ascending flows over the Indian subcontinent in the negative and positive phase of PDO
 464 coincided well with that in the La Niña and El Niño periods, respectively. Hence, PDO can significantly
 465 strengthen the effect of ENSO when they were in-phase.

466 **Table 3: List of individual and combined wintertime ENSO–PDO years during 1982–2014.**

Events	Phase	
	Positive	Negative
ENSO	1983, 1987, 1988, 1991, 1993–1995, 1998, 2003, 2005, 2007, 2010, 2015, 2016, 2019	1982, 1984–1986, 1989, 1996, 1997, 1999–2001, 2006, 2008, 2009, 2011, 2012, 2014
PDO	1981–1988, 1996–1998, 2001, 2003– 2006, 2010, 2014–2019	1989, 1991, 1995, 1999, 2000, 2002, 2008, 2009, 2011, 2012
ENSO×PDO	1983, 1987–1989, 1998–2000, 2003, 2005, 2008–2012	1982, 1984–1986, 1991, 1995–1997, 2001, 2006, 2014



R (Niño-3 & DUSMASS)	−0.71 (P<0.01)	−0.34 (P>0.1)
-------------------------	----------------	---------------

Table 3 revealed that most of years (8 out of 14) when ENSO and PDO were in-phase appeared in the second period, i.e., 2000, 2003, 2005, and 2008–2012. Meanwhile, most of years (8 out of 11) when ENSO and PDO were out of phase appeared in the first period, i.e., 1982, 1984–1986, 1991, 1995, 1996, and 1997. Simultaneously, the winter Niño-3 exhibited lower correlation with DUSMASS in the first period when most of ENSO years were accompanied with anti-phase PDO. In addition, the quantitative contribution of PDO shown in Fig. 12 further confirmed that the PDO strengthened the impact of ENSO on DUSMASS in 2000–2014 while the contribution was close to 0.0 in 1982–1996. All those demonstrated that the phase shift of PDO plays an important role in modulating the revolution of DUSMASS–Niño-3 relationship.

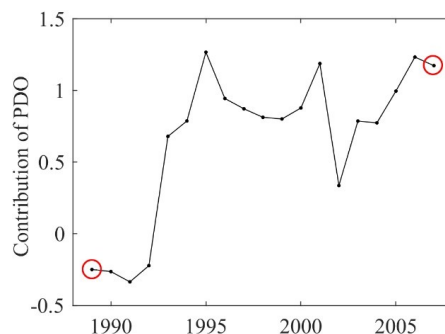


Figure 12: Sliding contribution of PDO to ENSO–DUSMASS relationship. The two circles represented the 15-year window spanning from 1982 to 1996 and 2000 to 2014, respectively.

4 Discussion

4.1 Uncertainty in analyzing the contribution of the influence factors

The schematic diagram of the interdecadal shift of the ENSO impact on DUSMASS was shown in Fig. S2. It illustrated that all the SSTA patterns in Atlantic Ocean, Pacific Ocean, and Indian Ocean play important roles in changing the ENSO–DUSMASS relationship. The contributions of those abovementioned factors to the interdecadal shift of this relationship were analyzed based on the linear regression model. However, the linear regression model would definitely bring uncertainty to the results (Guo et al., 2017) and may not be sufficient to verify the causal relationship between the factors and the ENSO–DUSMASS relationship. The numerical models are thus suggested to more accurately quantify



the contribution of those factors to the shift of ENSO–DUSMASS relationship, which will be included in our future research. However, it is undeniable that this study provides new sights to the dust storm-related numerical simulation by taking account of the teleconnections and their influence mechanisms.

In addition, while analyzing the effects of different types of ENSO event in Sect. 3.2.2, we compared the variance of the difference in SST over the tropical western Indian ocean between two adjacent months, as shown in Figs. 6, 7, and 9. It showed that only eight EP and EM ENSO years were identified and the number of CP and CT ENSO years were also insufficient. The statistical results acquired from the insufficient number of samples could also be explained by the random events (Pallikari, 2004). In order to verify this conclusion, we calculated the interannual correlation between the variance of SST difference and DUSMASS from 1982 to 2014. Even so, the significant interannual correlation does not guarantee the significant link between different types of ENSO. Therefore, longer time series with valid samples (EP, CP, CT, and EM ENSO years) are needed to further validate the influence of ENSO types on the ENSO–DUSMASS relationship in the future. Alternatively, using numerical model to simulate the teleconnection pattern of ENSO over South Asia under different types of ENSO is also favorable.

It is possible that the interdecadal variability of ENSO–DUSMASS relationship results from anthropogenic land-use management (Kumar et al., 1999), which should be considered in the future researches.

4.2 Difference in varied seasons and ENSO types

In this study, we analyzed the effect of wintertime ((–1) Nov.–(0) Jan.) ENSO on DUSMASS. It is noteworthy that the correlation between summertime ((–1) Jun.–(–1) Aug) ENSO and DUSMASS also exhibited remarkable interdecadal variability in the context of global warming, i.e., the correlation coefficient shifted from –0.24 ($P>0.1$) during 1982–1996 to –0.81 ($P<0.001$) during 2000–2014. It is known that lead-lag interaction and feedback are common among the large-scale atmospheric teleconnections, and the teleconnection pattern in other oceans usually lags behind the atmospheric circulation of Pacific Ocean (Trenbeth et al., 2002). Regarding this, the summertime ENSOs were obtained from the antecedent year, i.e., (–1) Jun.–(–1) Aug. The impact of summer and winter ENSO on the following summer DUSMASS would be confused when the lag effects were taken into account. Therefore, only wintertime ENSO impacts were displayed in this study, which could be the superimposed effects of summertime and wintertime ENSO. The precise numerical simulation is needed to further



517 isolate the seasonal difference in detail.

518 The CT ENSO refers to the summer ENSO that primarily starts from the preceding winter, whereas
519 the EM ENSO refers to the ENSO event that emerges in late spring (Yang and Huang, 2021). Similarly,
520 the onset of EP ENSOs tends to occur in spring while that of CP ENSOs appear in summer. Besides, both
521 CT and EP ENSOs dominate in 1979–1997, while the EM and CP ENSOs become more frequent in
522 2000–2018 (Kao and Yu, 2009; Yang and Huang, 2021). Thus, it is likely that the CT (EM) ENSOs may
523 coincide with EP (CP) ENSOs. However, the years defined as CT (EM) ENSO years using Yang and
524 Huang (2021)’s method were not consistent with the EP (CP) ENSO years and they were crossed among
525 different types of ENSOs, indicating that the CT (EM) ENSOs were independent of the EP (CP) ENSOs.
526 Yang and Huang (2021) suggested that the impact of ENSO on ISMR is significant when EM ENSOs
527 dominated, while it is weak when CT ENSOs prevailed. It is further demonstrated that the transition of
528 EP and CP ENSO exhibits no significant contribution to the shift of relationship between ISMR and
529 ENSO since the 21st century. Those are also true for the revolution of ENSO–DUSMASS relationship.

530 **5 Conclusions**

531 In the study, we investigated the interdecadal change of the ENSO impact on DUSMASS over the
532 northwestern South Asia from 1982 to 2014 as well as factors that contribute to the shifts of the responses
533 of DUSMASS to the wintertime ENSO. It was found that the ENSO–DUSMASS relationship shifted
534 from weak negative relation during 1982–1996 to significant negative correlation during 2000–2014.
535 The change of Atlantic SSTA pattern weakened the impact of wintertime ENSO on dust activities over
536 the northwestern South Asia, while that of Indian Ocean SSTA pattern and PDO tended to strengthen
537 ENSO’s effect. Both the Atlantic and Indian Ocean SSTA patterns were modulated by the duration of
538 ENSO events (i.e., continuing and emerging ENSO). The Eurasian continent and Indian Ocean thermal
539 contrast cannot explain the shift of ENSO–DUSMASS relationship. The current results are based solely
540 on the linear regression, and further studies integrating numerical models and longer time series are
541 needed to validate the results. Nevertheless, our study indeed found multiple large-scale factors that could
542 impact the interdecadal interaction between ENSO and dust activities over the northwestern South Asia.
543 Considering the large-scale circulation forecast is relatively easier, the results in this study could provide
544 new insight to the prediction of dust storm trend in the near future based on the variability of ENSO–



545 DUSMASS relationship.

546 **Data availability**

547 The data can be downloaded for free from the corresponding website which were listed in the text.

548 **Author contribution**

549 L.S. designed the study, performed the analysis with feedback from J.Z. and F.Y., and wrote the
550 paper that was reviewed by J.Z., F.Y., D.Z., J.W., X.M., and Y.L.. All the authors discussed the results.

551 **Competing interests**

552 The authors declare that they have no conflict of interest.

553 **Acknowledgments**

554 The authors would like to thank the Modern-Era Retrospective Analysis for Research and
555 Applications, version 2 (MERRA-2) for providing the surface dust mass concentration, wind speed and
556 planetary boundary layer height, the National Oceanic and Atmospheric Administration (NOAA) for
557 providing the SST, the Hadley Centre Climate Research Unit for the land-surface temperature and
558 precipitation, the National Aeronautics and Space Administration (NASA) for the NDVI, and the Climate
559 Predict Center of National Oceanic and Atmospheric Administration (NOAA/CPC) for the large-scale
560 climate indices.

561 This work was supported by the Strategic Priority Research Program of the Chinese Academy of
562 Sciences-A (No. XDA19030402) and the National Natural Science Foundation of China (No. 42071425).

563 **References**

- 564 Agrawal, N., Pandey, V. K. and Shahi, N. K.: Enso-Iod Changing Relationship and Its Impact on Indian
565 Summer Monsoon Rainfall, Int. J. Tech. Non-Technical Res., 8(5), 165–174, 2017.
- 566 Augustyn, A., Zeidan, A., Zelazko, A., Eldridge, A., McKenna, A., Tikkanen, A., Gadzikowski, A.,
567 Schreiber, B. A., Duignan, B., Mahajan, D., Promeet, D., Goldstein, E. and Rodriguez, E.: Thar
568 Desert, Encycl. Br. [online] Available from: <https://www.britannica.com/place/Thar-Desert>, 2019.



- 569 Avila, A.: The chemical composition of dust transported in red rains—its contribution to the
 570 biogeochemical cycle of a holm oak forest in Catalonia (Spain), *Atmos. Environ.*, 32(2), 179–191,
 571 1998.
- 572 Banerjee, P. and Kumar, S. P.: ENSO modulation of interannual variability of dust aerosols over the
 573 northwest Indian Ocean, *J. Clim.*, 29(4), 1391–1415, doi:10.1175/JCLI-D-15-0039.1, 2016.
- 574 Banerjee, P., Satheesh, S. K., Moorthy, K. K., Nanjundiah, R. S. and Nair, V. S.: Long-range transport
 575 of mineral dust to the northeast Indian Ocean: Regional versus remote sources and the implications,
 576 *J. Clim.*, 32(5), 1525–1549, doi:10.1175/JCLI-D-18-0403.1, 2019.
- 577 Banerjee, P., Satheesh, S. K. and Krishna Moorthy, K.: Is the Atlantic Ocean driving the recent variability
 578 in South Asian dust?, *Atmos. Chem. Phys.*, 21(23), 17665–17685, doi:10.5194/acp-2020-1305, 2021.
- 579 Behrooz, R. D., Esmaili-Sari, A., Bahramifar, N. and Kaskaoutis, D. G.: Analysis of the TSP, PM10
 580 concentrations and water-soluble ionic species in airborne samples over Sistan, Iran during the
 581 summer dusty period, *Atmos. Pollut. Res.*, 8(3), 403–417, 2017.
- 582 Bollasina, M. A., Ming, Y. and Ramaswamy, V.: Anthropogenic aerosols and the weakening of the south
 583 asian summer monsoon, *Science* (80-.), 334(6055), 502–505, doi:10.1126/science.1204994, 2011.
- 584 Bozlaker, A., Prospero, J. M., Fraser, M. P. and Chellam, S.: Quantifying the contribution of long-range
 585 saharan dust transport on particulate matter concentrations in Houston, Texas, using detailed
 586 elemental analysis, *Environ. Sci. Technol.*, 47(18), 10179–10187, doi:10.1021/es4015663, 2013.
- 587 Cai, W., Borlace, S., Lengaigne, M., Van Rensch, P., Collins, M., Vecchi, G., Timmermann, A., Santoso,
 588 A., Mcphaden, M. J., Wu, L., England, M. H., Wang, G., Guilyardi, E. and Jin, F. F.: Increasing
 589 frequency of extreme El Niño events due to greenhouse warming, *Nat. Clim. Chang.*, 4(2), 111–116,
 590 doi:10.1038/nclimate2100, 2014.
- 591 Chauhan, S. S.: Desertification control and management of land degradation in the Thar desert of India,
 592 *Environmentalist*, 23(3), 219–227, doi:10.1023/B:ENVR.0000017366.67642.79, 2003.
- 593 Chen, Y.-S., Sheen, P.-C., Chen, E.-R., Liu, Y.-K., Wu, T.-N. and Yang, C.-Y.: Effects of Asian dust
 594 storm events on daily mortality in Taipei, Taiwan., *Environ. Res.*, 95(2), 151–155,
 595 doi:10.1016/j.envres.2003.08.008, 2004.
- 596 Clark, C. O., Cole, J. E. and Webster, P. J.: Indian Ocean SST and Indian summer rainfall: Predictive
 597 relationships and their decadal variability, *J. Clim.*, 13(14), 2503–2519, doi:10.1175/1520-
 598 0442(2000)013<2503:IOSAIS>2.0.CO;2, 2000.



- 599 Colarco, P., Da Silva, A., Chin, M. and Diehl, T.: Online simulations of global aerosol distributions in
 600 the NASA GEOS-4 model and comparisons to satellite and ground-based aerosol optical depth, J.
 601 Geophys. Res. Atmos., 115, D14207, doi:10.1029/2009JD012820, 2010.
- 602 Deser, C., Guo, R. and Lehner, F.: The relative contributions of tropical Pacific sea surface temperatures
 603 and atmospheric internal variability to the recent global warming hiatus, Geophys. Res. Lett., 44(15),
 604 7945–7954, doi:10.1002/2017GL074273, 2017.
- 605 Dong, B., Dai, A., Vuille, M. and Timm, O. E.: Asymmetric modulation of ENSO teleconnections by
 606 the interdecadal Pacific oscillation, J. Clim., 31(18), 7337–7361, doi:10.1175/JCLI-D-17-0663.1,
 607 2018.
- 608 Easterling, D. R. and Wehner, M. F.: Is the climate warming or cooling?, Geophys. Res. Lett., 36(8), 4–
 609 6, doi:10.1029/2009GL037810, 2009.
- 610 Erel, Y., Dayan, U., Rabi, R., Rudich, Y. and Stein, M.: Trans boundary transport of pollutants by
 611 atmospheric mineral dust, Environ. Sci. Technol., 40(9), 2996–3005, doi:10.1021/es0515021, 2006.
- 612 Fyfe, J. C., Merryfield, W. J., Kharin, V., Boer, G. J., Lee, W. S. and Von Salzen, K.: Skillful predictions
 613 of decadal trends in global mean surface temperature, Geophys. Res. Lett., 38(22), 1–5,
 614 doi:10.1029/2011GL049508, 2011.
- 615 Fyfe, J. C., Gillett, N. P. and Zwiers, F. W.: Overestimated global warming over the past 20 years, Nat.
 616 Clim. Chang., 3(9), 767–769, doi:10.1038/nclimate1972, 2013.
- 617 Gelaro, R., McCarty, W., Suárez, M. J., Todling, R., Molod, A., Takacs, L., Randles, C. A., Darmenov,
 618 A., Bosilovich, M. G., Reichle, R., Wargan, K., Coy, L., Cullather, R., Draper, C., Akella, S., Buchard,
 619 V., Conaty, A., da Silva, A. M., Gu, W., Kim, G. K., Koster, R., Lucchesi, R., Merkova, D., Nielsen,
 620 J. E., Partyka, G., Pawson, S., Putman, W., Rienecker, M., Schubert, S. D., Sienkiewicz, M. and Zhao,
 621 B.: The modern-era retrospective analysis for research and applications, version 2 (MERRA-2), J.
 622 Clim., 30(14), 5419–5454, doi:10.1175/JCLI-D-16-0758.1, 2017.
- 623 Ginoux, P., Chin, M., Tegen, I., Prospero, J. M., Holben, B., Dubovik, O. and Lin, S.-J.: Sources and
 624 distributions of dust aerosols simulated with the GOCART model, J. Geophys. Res. Atmos.,
 625 106(D17), 20255–20273, doi:10.1029/2000JD000053, 2001.
- 626 Graham, N. E.: Decadal-scale climate variability in the tropical and North Pacific during the 1970s and
 627 1980s: observations and model results, Clim. Dyn., 10(3), 135–162, doi:10.1007/BF00210626, 1994.
- 628 Guo, H., Wang, X. and Gao, Z.: Uncertain linear regression model and its application, J. Intell. Manuf.,



- 28(3), 559–564, doi:10.1007/s10845-014-1022-4, 2017.
- He, L., Lin, A., Chen, X., Zhou, H., Zhou, Z. and He, P.: Assessment of MERRA-2 Surface PM_{2.5} over the Yangtze River Basin: Ground-based verification, spatiotemporal distribution and meteorological dependence, *Remote Sens.*, 11(4), 460, doi:10.3390/rs11040460, 2019.
- Hirahara, S., Ishii, M. and Fukuda, Y.: Centennial-scale sea surface temperature analysis and its uncertainty, *J. Clim.*, 27(1), 57–75, doi:10.1175/JCLI-D-12-00837.1, 2014.
- Hu, H., Wu, Q. and Wu, Z.: Influences of two types of El Niño event on the Northwest Pacific and tropical Indian Ocean SST anomalies, *J. Oceanol. Limnol.*, 36(1), 33–47, doi:10.1007/s00343-018-6296-5, 2018.
- Hu, S. and Fedorov, A. V.: The extreme El Niño of 2015–2016 and the end of global warming hiatus, *Geophys. Res. Lett.*, 44(8), 3816–3824, doi:10.1002/2017GL072908, 2017.
- Hu, Z. Z., Kumar, A., Jha, B., Wang, W., Huang, B. and Huang, B.: An analysis of warm pool and cold tongue El Niños: Air-sea coupling processes, global influences, and recent trends, *Clim. Dyn.*, 38(9–10), 2017–2035, doi:10.1007/s00382-011-1224-9, 2012.
- Huang, X., Zhou, T., Turner, A., Dai, A., Chen, X., Clark, R., Jiang, J., Man, W., Murphy, J., Rostron, J., Wu, B., Zhang, L., Zhang, W. and Zou, L.: The recent decline and recovery of Indian summer monsoon rainfall: Relative roles of external forcing and internal variability, *J. Clim.*, 33(12), 5035–5060, doi:10.1175/JCLI-D-19-0833.1, 2020.
- Jin, Q. and Wang, C.: The greening of Northwest Indian subcontinent and reduction of dust abundance resulting from Indian summer monsoon revival, *Sci. Rep.*, 8(1), 1–9, doi:10.1038/s41598-018-23055-5, 2018.
- Jin, Q., Wei, J., Pu, B., Yang, Z. L. and Parajuli, S. P.: High Summertime Aerosol Loadings Over the Arabian Sea and Their Transport Pathways, *J. Geophys. Res. Atmos.*, 123(18), 10,568–10,590, doi:10.1029/2018JD028588, 2018.
- Kaiser, J. and Granmar, M.: Mounting Evidence Indicts Fine-Particle Pollution, *Science* (80-.), 307(5717), 1858–1861, 2005.
- Kao, H. Y. and Yu, J. Y.: Contrasting Eastern-Pacific and Central-Pacific types of ENSO, *J. Clim.*, 22(3), 615–632, doi:10.1175/2008JCLI2309.1, 2009.
- Kinter, I. L., Miyakoda, K. and Yang, S.: Recent change in the connection from the Asian monsoon to ENSO, *J. Clim.*, 15(10), 1203–1215, doi:10.1175/1520-0442(2002)015<1203:RCITCF>2.0.CO;2,



- 2002.
- Kosaka, Y. and Xie, S. P.: Recent global-warming hiatus tied to equatorial Pacific surface cooling, *Nature*, 501(7467), 403–407, doi:10.1038/nature12534, 2013.
- Kosaka, Y. and Xie, S. P.: The tropical Pacific as a key pacemaker of the variable rates of global warming, *Nat. Geosci.*, 9(9), 669–673, doi:10.1038/ngeo2770, 2016.
- Krishnamurthy, L. and Krishnamurthy, V.: Influence of PDO on South Asian summer monsoon and monsoon-ENSO relation, *Clim. Dyn.*, 42(9–10), 2397–2410, doi:10.1007/s00382-013-1856-z, 2014.
- Krishnamurthy, V. and Kirtman, B. P.: Variability of the Indian Ocean: Relation to monsoon and ENSO, *Q. J. R. Meteorol. Soc.*, 129(590), 1623–1646, doi:10.1256/qj.01.166, 2003.
- Kucharski, F. and Joshi, M. K.: Influence of tropical South Atlantic sea-surface temperatures on the Indian summer monsoon in CMIP5 models, *Q. J. R. Meteorol. Soc.*, 143(704), 1351–1363, doi:10.1002/qj.3009, 2017.
- Kucharski, F., Bracco, A., Yoo, J. H. and Molteni, F.: Low-frequency variability of the Indian monsoon-ENSO relationship and the tropical Atlantic: The “weakening” of the 1980s and 1990s, *J. Clim.*, 20(16), 4255–4266, doi:10.1175/JCLI4254.1, 2007.
- Kucharski, F., Bracco, A., Yoo, J. H. and Molteni, F.: Atlantic forced component of the Indian monsoon interannual variability, *Geophys. Res. Lett.*, 35(4), 1–5, doi:10.1029/2007GL033037, 2008.
- Kucharski, F., Bracco, A., Yoo, J. H., Tompkins, A. M., Feudale, L., Ruti, P. and Dell’Aquila, A.: A Gill-Matsuno-type mechanism explains the tropical Atlantic influence on African and Indian monsoon rainfall, *Q. J. R. Meteorol. Soc.*, 135(640), 569–579, doi:10.1002/qj.406, 2009.
- Kug, J. S., An, S. Il, Jin, F. F. and Kang, I. S.: Preconditions for El Niño and La Niña onsets and their relation to the Indian Ocean, *Geophys. Res. Lett.*, 32(5), 1–5, doi:10.1029/2004GL021674, 2005.
- Kumar, K. K., Rajagopalan, B. and Cane, M. A.: On the weakening relationship between the Indian monsoon and ENSO, *Science* (80-.), 284(5423), 2156–2159, doi:10.1126/science.284.5423.2156, 1999.
- Kumar, K. K., Rajagopalan, B., Hoerling, M., Bates, G. and Cane, M.: Unraveling the mystery of Indian monsoon failure during El Niño, *Science* (80-.), 314(5796), 115–119, doi:10.1126/science.1131152, 2006.
- Li, T., Zhang, Y., Lu, E. and Wang, D.: Relative role of dynamic and thermodynamic processes in the development of the Indian Ocean dipole: An OGCM diagnosis, *Geophys. Res. Lett.*, 29(23),



- doi:10.1029/2002GL015789, 2002.
- Mahowald, N. M., Kloster, S., Engelstaedter, S., Moore, J. K., Mukhopadhyay, S., McConnell, J. R., Albani, S., Doney, S. C., Bhattacharya, A., Curran, M. A. J., Flanner, M. G., Hoffman, F. M., Lawrence, D. M., Lindsay, K., Mayewski, P. A., Neff, J., Rothenberg, D., Thomas, E., Thornton, P. E. and Zender, C. S.: Observed 20th century desert dust variability: Impact on climate and biogeochemistry, *Atmos. Chem. Phys.*, 10(22), 10875–10893, doi:10.5194/acp-10-10875-2010, 2010.
- McPhaden, M. J., Lee, T. and McClurg, D.: El Niño and its relationship to changing background conditions in the tropical Pacific Ocean, *Geophys. Res. Lett.*, 38(15), doi:10.1029/2011GL048275, 2011.
- Nitta, T. and Yamada, S.: Recent warming of tropical sea surface temperature and its relationship to the Northern Hemisphere circulation, *J. Meteorol. Soc. Japan*, 67(3), 375–383, doi:10.2151/jmsj1965.67.3_375, 1989.
- Osborn, T. J., Jones, P. D., Lister, D. H., Morice, C. P., Simpson, I. R., Winn, J. P., Hogan, E. and Harris, I. C.: Land Surface Air Temperature Variations Across the Globe Updated to 2019: The CRUTEM5 Data Set, *J. Geophys. Res. Atmos.*, 126(2), doi:10.1029/2019JD032352, 2021.
- Pallikari, F.: On the false hypothesis of psi-mediated shift of statistical average in tests with random number generators, in *The Parapsychological Association Convention 2004*, pp. 157–171., 2004.
- Parker, D. J., Willetts, P., Birch, C., Turner, A. G., Marsham, J. H., Taylor, C. M., Kolusu, S. and Martin, G. M.: The interaction of moist convection and mid-level dry air in the advance of the onset of the Indian monsoon, *Q. J. R. Meteorol. Soc.*, 142(699), 2256–2272, doi:10.1002/qj.2815, 2016.
- Poulsen, O. M., Breum, N. O., Ebbehøj, N., Hansen, A. M., Ivens, U. I., van Lelieveld, D., Malmros, P., Matthiasen, L., Nielsen, B. H. and Nielsen, E. M.: Sorting and recycling of domestic waste. Review of occupational health problems and their possible causes., *Sci. Total Environ.*, 168(1), 33–56, 1995.
- Randles, C. A., Sliva, A. M. da, Buchard, V., Colarco, P., Armenov, A. and Govindaraju, R.: The MERRA-2 Aerosol Reanalysis, 1980 Onward. Part I: System Description and Data Assimilation Evaluation, *J. Clim.*, 30(17), 6823–6850, doi:10.1175/JCLI-D-16-0609.1, 2017.
- Rayner, N. A., Parker, D. E., Horton, E. B., Folland, C. K., Alexander, L. V., Rowell, D. P., Kent, E. C. and Kaplan, A.: Global analyses of sea surface temperature, sea ice, and night marine air temperature since the late nineteenth century, *J. Geophys. Res. Atmos.*, 108(D14), 4407,



- 719 doi:10.1029/2002jd002670, 2003.
- 720 Razakov, R. M. and Kosnazarov, K. A.: Dust and salt transfer from the exposed bed of the Aral Sea and
 721 measures to decrease its environmental impact, in *The Aral Sea Basin*, edited by P. P. Micklin and
 722 W. D. Williams, pp. 95–102, Springer, Berlin, Heidelberg, 1996.
- 723 Richon, C., Dutay, J., Dulac, F. and Wang, R.: Modeling the biogeochemical impact of atmospheric
 724 phosphate deposition from desert dust and combustion sources to the Mediterranean Sea,
 725 *Biogeosciences*, 15(8), 2499–2524, doi:10.5194/bg-2017-242, 2018.
- 726 Rienecker, M. M., Suarez, M. J., Gelaro, R., Todling, R., Bacmeister, J., Liu, E., Bosilovich, M. G.,
 727 Schubert, S. D., Takacs, L., Kim, G. K., Bloom, S., Chen, J., Collins, D., Conaty, A., Da Silva, A.,
 728 Gu, W., Joiner, J., Koster, R. D., Lucchesi, R., Molod, A., Owens, T., Pawson, S., Pegion, P., Redder,
 729 C. R., Reichle, R., Robertson, F. R., Ruddick, A. G., Sienkiewicz, M. and Woollen, J.: MERRA:
 730 NASA’s modern-era retrospective analysis for research and applications, *J. Clim.*, 24(14), 3624–
 731 3648, doi:10.1175/JCLI-D-11-00015.1, 2011.
- 732 Rong, X. Y., Zhang, R. H. and Li, T.: Impacts of Atlantic sea surface temperature anomalies on Indo-
 733 East Asian summer monsoon-ENSO relationship, *Chinese Sci. Bull.*, 55(22), 2458–2468,
 734 doi:10.1007/s11434-010-3098-3, 2010.
- 735 Roy, S. Sen, Goodrich, G. B. and Balling, R. C.: Influence of El Niño/southern oscillation, Pacific
 736 decadal oscillation, and local sea-surface temperature anomalies on peak season monsoon
 737 precipitation in India, *Clim. Res.*, 25(2), 171–178, doi:10.3354/cr025171, 2003.
- 738 Sabeerali, C. T., Ajayamohan, R. S., Bangalath, H. K. and Chen, N.: Atlantic Zonal Mode: An Emerging
 739 Source of Indian Summer Monsoon Variability in a Warming World, *Geophys. Res. Lett.*, 46(8),
 740 4460–4467, doi:10.1029/2019GL082379, 2019.
- 741 Sanchez de la Campa, A., Garcia-Salamanca, A., Solano, J., de la Rosa, J. and Ramos, J.-L.: Chemical
 742 and microbiological characterization of atmospheric particulate matter during an intense African dust
 743 event in Southern Spain., *Environ. Sci. Technol.*, 47(8), 3630–3638, doi:10.1021/es3051235, 2013.
- 744 Schulz, M., Prospero, J. M., Baker, A. R., Dentener, F., Ickes, L., Liss, P. S., Mahowald, N. M., Nickovic,
 745 S., García-Pando, C. P., Rodríguez, S., Sarin, M., Tegen, I. and Duce, R. A.: Atmospheric Transport
 746 and Deposition of Mineral Dust to the Ocean: Implications for Research Needs, *Environ. Sci.*
 747 *Technol.*, 46(19), 10390–10404, doi:10.1021/es300073u, 2012.
- 748 Singh, R. P., Prasad, A. K., Kayetha, V. K. and Kafatos, M.: Enhancement of oceanic parameters



- 749 associated with dust storms using satellite data, *J. Geophys. Res.*, 113, C11008,
 750 doi:10.1029/2008JC004815, 2008.
- 751 Srivastava, G., Chakraborty, A. and Nanjundiah, R. S.: Multidecadal see-saw of the impact of ENSO on
 752 Indian and West African summer monsoon rainfall, *Clim. Dyn.*, 52(11), 6633–6649,
 753 doi:10.1007/s00382-018-4535-2, 2019.
- 754 Storch, H. von and Zwiers, F. W.: *Statistical Analysis in Climate Research*, Cambridge University Press,
 755 Cambridge., 1999.
- 756 Tokinaga, H., Richter, I. and Kosaka, Y.: ENSO Influence on the Atlantic Niño, Revisited: Multi-Year
 757 versus Single-Year ENSO Events, *J. Clim.*, 32(14), 4585–4600, 2019.
- 758 Trenberth, K. E. and Hurrell, J. W.: Decadal atmosphere-ocean variations in the Pacific, *Clim. Dyn.*, 9(6),
 759 303–319, doi:10.1007/BF00204745, 1994.
- 760 Trenberth, K. E., Dai, A., Van Der Schrier, G., Jones, P. D., Barichivich, J., Briffa, K. R. and Sheffield,
 761 J.: Global warming and changes in drought, *Nat. Clim. Chang.*, 4(1), 17–22,
 762 doi:10.1038/nclimate2067, 2014.
- 763 Trenbeth, K. E., Caron, J. M., Stepaniak, D. P. and Worley, S.: Evolution of El Niño-Southern Oscillation
 764 and global atmospheric surface temperatures, *J. Geophys. Res. D Atmos.*, 107(7–8), 5–1,
 765 doi:10.1029/2000jd000298, 2002.
- 766 Veselovskii, I., Goloub, P., Podvin, T., Tanre, D., Da Silva, A., Colarco, P., Castellanos, P., Korenskiy,
 767 M., Hu, Q., Whiteman, D. N., Pérez-Ramírez, D., Augustin, P., Fourmentin, M. and Kolgotin, A.:
 768 Characterization of smoke and dust episode over West Africa: Comparison of MERRA-2 modeling
 769 with multiwavelength Mie-Raman lidar observations, *Atmos. Meas. Tech.*, 11(2), 949–969,
 770 doi:10.5194/amt-11-949-2018, 2018.
- 771 Wang, B., Wu, R. and Li, T.: Atmosphere-warm ocean interaction and its impacts on Asian-Australian
 772 monsoon variation, *J. Clim.*, 16(8), 1195–1211, doi:10.1175/1520-
 773 0442(2003)16<1195:AOIAII>2.0.CO;2, 2003.
- 774 Watanabe, M. and Jin, F. F.: Role of Indian Ocean warming in the development of Philippine Sea
 775 anticyclone during ENSO, *Geophys. Res. Lett.*, 29(10), 1161–1164, doi:10.1029/2001gl014318,
 776 2002.
- 777 Watanabe, M., Shiogama, H., Tatebe, H., Hayashi, M., Ishii, M. and Kimoto, M.: Contribution of natural
 778 decadal variability to global warming acceleration and hiatus, *Nat. Clim. Chang.*, 4(10), 893–897,



- 779 doi:10.1038/nclimate2355, 2014.
- 780 Wu, R. and Kirtman, B. P.: Understanding the impacts of the Indian ocean on ENSO variability in a
 781 coupled GCM, J. Clim., 17(20), 4019–4031, doi:10.1175/1520-
 782 0442(2004)017<4019:UTIOI>2.0.CO;2, 2004.
- 783 Yadav, R. K.: Changes in the large-scale features associated with the Indian summer monsoon in the
 784 recent decades, *Int. J. Climatol.*, 29, 117–133, doi:10.1002/joc, 2009.
- 785 Yadav, R. K.: On the relationship between east equatorial Atlantic SST and ISM through Eurasian wave,
 786 *Clim. Dyn.*, 48, 281–295, doi:10.1007/s00382-016-3074-y, 2016.
- 787 Yadav, R. K., Srinivas, G. and Chowdary, J. S.: Atlantic Niño modulation of the Indian summer monsoon
 788 through Asian jet, *npj Clim. Atmos. Sci.*, 1(1), doi:10.1038/s41612-018-0029-5, 2018.
- 789 Yang, X. and Huang, P.: Restored relationship between ENSO and Indian summer monsoon rainfall
 790 around 1999/2000, *Innov.*, 2(2), 100102, doi:10.1016/j.xinn.2021.100102, 2021.
- 791 Yeh, S. W., Kug, J. S., Dewitte, B., Kwon, M. H., Kirtman, B. P. and Jin, F. F.: El Nino in a changing
 792 climate, *Nature*, 461(7263), 511–514, doi:10.1038/nature08316, 2009.
- 793 Yu, J.-Y., Mechoso, C. R., McWilliams, J. C. and Arakawa, A.: Impacts of the Indian Ocean on the
 794 ENSO cycle, *Geophys. Res. Lett.*, 29(8), 1204, 2002.
- 795 Yu, Y., Notaro, M., Liu, Z., Wang, F., Alkolibi, F., Fadda, E. and Bakhrjy, F.: Climatic controls on the
 796 interannual to decadal variability in Saudi Arabian dust activity: Toward the development of a
 797 seasonal dust prediction model, *J. Geophys. Res. Atmos.*, 120(5), 1739–1758,
 798 doi:10.1002/jgrc.20224, 2015.
- 799 Zhang, J. and Reid, J. S.: An analysis of clear sky and contextual biases using an operational over ocean
 800 MODIS aerosol product, *Geophys. Res. Lett.*, 36(15), L15824, doi:10.1029/2009GL038723, 2009.
- 801